Supporting Material

Tubulin Polarizability in Aqueous Suspensions

Jose Rafael Guzman-Sepulveda[1], Ruitao Wu[1], Aarat Kalra[2], Maral Aminpour[2], Jack Tuszynski[2,3,4], and Aristide Dogariu[1*]

[1] *CREOL, The College of Optics and Photonics, University of Central Florida, USA*

[2] *Department of Physics, University of Alberta, Canada.*

[3] *Department of Oncology, University of Alberta, Canada.*

[4] *Department of Mechanical and Aerospace Engineering, Politecnico di Torino, Italy*

**Corresponding author: adogariu@creol.ucf.edu*

Appendix A – Detailed sample preparation

The tubulin samples were prepared mainly by following the standard protocol from Cytoskeleton, Inc., similarly to previous reports [1]. Before the sample preparation, BRB80 buffer (also known as general tubulin buffer, containing 80 mM PIPES pH 6.9, 2 mM $MgCl_2$ and 0.5 mM EGTA, acquired from Cytoskeleton, Inc.) was filtered to remove aggregates (0.22 µm pore size). The so-called cushion buffer solution consists of a mixture of glycerol (60 vol%) and pre-filtered BRB80 buffer (40 vol%). These two buffers were stored at 0°C and used within 6 months after preparation.

Before reconstitution, GTP (BST06-010, Cytoskeleton, Inc.) was added to the pre-filtered BRB80 buffer. The resulting solution, called G-PEM buffer, contains 1mM GTP. The tubulin suspension was reconstituted in ice from pure tubulin (porcine brain, >99% pure, T240, Cytoskeleton, Inc.) using a mixture of cushion buffer (10%) and G-PEM buffer (90%). Thus, the reconstituted tubulin suspension contains 5 mg/ml tubulin and 6 % of glycerol.

Next, 20 µM colchicine (≥95% (HPLC), powder, C9754 Sigma) was added into the reconstituted suspension to further inhibit the polymerization and aggregation of tubulin dimers. Different concentration of tubulin in the suspension was obtain by diluting the above concentrated suspension with pre-filtered BRB80 buffer. Once finished, the sample was kept in ice and the measurement was carried out within 6 hours after preparation.

We note that the sample preparation is not trivial considering the possible polymerization and aggregation of tubulin dimers. Three steps should be highlighted in our preparation that were implemented specifically to minimize these effects. First, the sample should be prepared at 0 °C and used immediately after the preparation. Second, glycerol should be added in the suspension to slow down the aggregation of tubulin dimers by increasing the viscosity of the solvent. Finally, colchicine was added to prevent the tubulin dimers from both polymerization and aggregation. The optical purity of the sample was verified using bout our coherence-gated DLS and a standard DLS (Malvern Zetasizer).

Appendix B – Errors, errors propagation, and detailed discussion of the results

In terms of the EMT variables, the RI of the solute is a function of the volume fraction, the effective RI measured, and the (known) RI of the solvent i.e., $n_p \rightarrow n_p(\phi, n_{eff}, n_2)$, irrespectively of the EMT of choice. The specific functional form of $n_p(\phi, n_{eff}, n_2)$ is determined by the homogenization approach selected. The variational analysis for n_p in general leads to:

$$dn_p = \frac{\partial n_p}{\partial \phi} d\phi \; + \; \frac{\partial n_p}{\partial n_{eff}} dn_{eff} \; + \; \frac{\partial n_p}{\partial n_2} dn_2$$

Where the partial derivatives indicate the sensitivity of a variation in n_p due to changes in the volume fraction, the effective RI measured, and the RI of the solvent, respectively. In the simpler case where the effective medium changes only by variations of the volume fraction of particulates i.e., invariant solvent (n_2 is constant). Eq. (x) simplifies to:

$$dn_p = \frac{\partial n_p}{\partial \phi} d\phi \; + \; \frac{\partial n_p}{\partial n_{eff}} dn_{eff}$$

In this equation, the first term relates to both EMT and the sample preparation, and the second one to EMT and the measurement precision. Additionally, one can write explicitly the variation of the effective RI measured as $dn_{eff} = \frac{\partial n_{eff}}{\partial X} dX$, with respect to the experimental variable X used to measure n_{eff}.

$$dn_p = \frac{\partial n_p}{\partial \phi} d\phi + \frac{\partial n_p}{\partial n_{eff}} \; \frac{\partial n_{eff}}{\partial X} dX$$

In traditional refractometry, for instance, where n_{eff} is estimated from angles of TIR, the previous expression becomes $dn_p = \frac{\partial n_p}{\partial \phi} d\phi + \frac{\partial n_p}{\partial n_{eff}} \frac{\partial n_{eff}}{\partial \theta} d\theta$.

As mentioned, different optical mixing rules have been developed. The most commonly used are listed in Table S1. These are applied in different conditions, and some of them are based on mixing dipole theory while the others are empirical.

Table S1: Different models used for homogenization in effective medium theory

EMT model	Formula	Remarks	Ref
Maxwell Garnett	$\varepsilon_{eff} = \varepsilon_s + 3f\varepsilon_s \frac{\varepsilon_d - \varepsilon_s}{\varepsilon_d + 2\varepsilon_s - f(\varepsilon_d - \varepsilon_s)}$	Derivation start from macroscopic Maxwell's equations. Assumed spherical objects.	2
Lorentz-Lorenz	$\frac{\varepsilon_{eff} - 1}{\varepsilon_{eff} + 2} = (1 - f)\frac{\varepsilon_s - 1}{\varepsilon_s + 2} + f\frac{\varepsilon_d - 1}{\varepsilon_d + 2}$	Derivation based weak dipole-dipole interaction.	3
Wiener	$\frac{\varepsilon_{eff} - \varepsilon_s}{\varepsilon_{eff} + 2\varepsilon_s} = f\frac{\varepsilon_d - \varepsilon_s}{\varepsilon_d + \varepsilon_s}$	Similar to Lorentz rules. But good for small volume refraction.	4
Arago-Biot	$\varepsilon_{eff}^{1/2} = (1 - f)\varepsilon_s^{1/2} + f\varepsilon_d^{1/2}$	Empirical equation. Usually used for liquids.	5

To put the models in Table S1 in perspective, we plotted the effective refractive index estimated from different EMT, for a mixture of water and tubulin (using the permittivity measured in this work) in the full range of volume fractions (Figure S1(a)) and the dilute limit (Figure S1(b)). The latter actually corresponds to the concentration range in this work.

In the range of concentration explored here (dilute limit; volume fraction $\lesssim$0.003), all the effective refractive index using different EMT explored behave linearly with an acceptable degree of accuracy (see Figure S1(b)). This linear behavior in this range of tubulin concentration may serve as justification to as why a number of reports addressing similar measurements on protein suspensions use a linear model directly (Arago-Biot). In our case, we used the Maxwell-Garnett model to account for any small possible deviation from the linear behavior.

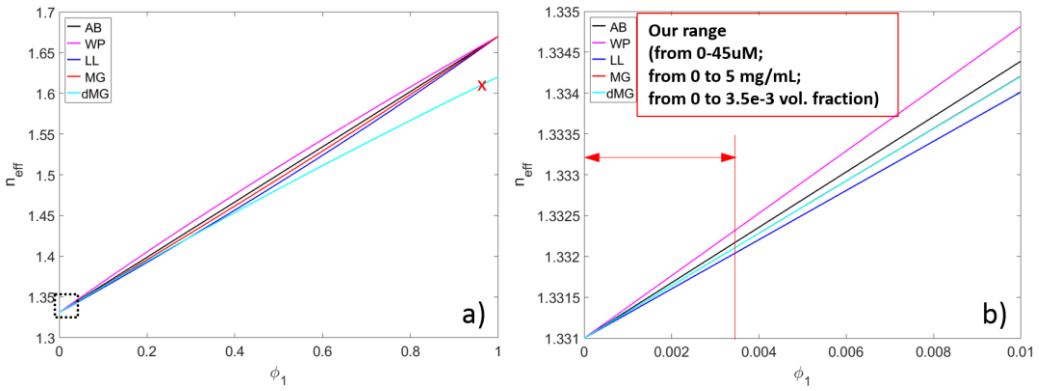

Figure S1. Effective refractive index of a mixture of water and tubulin, as a function of the volume fraction of tubulin, estimated from different EMT for a) the full range of possible volume fractions, and b) the dilute limite ($\phi \leq 1 \times 10^{-2}$). The labels refer to the abbreviations of the different EMT: Arago-Biot (AB); Wiener (WP); Lorentz-Lorentz (LL); Maxwell-Garnett (MG), and dilurte approximation of Maxwell-Garnett (dMG). The concentration range in our work is indicated in panel (b).

***Error propagation in the AB model*.** In the recent reports on the RI of tubulin in suspension [1, 6] the Arago-Biot model, $n_{eff} = (1-\phi)n_2 + \phi n_p$, was used. Within the frame of this model, the RI of the inclusions retrieved reads as $n_p(\phi, n_{eff}, n_2) = \frac{1}{\phi}\left(n_{eff} - (1-\phi)n_2\right)$, from which the sensitivity terms can be evaluated as:

$$\frac{\partial n_p}{\partial n_{eff}} = \frac{1}{\phi}$$

$$\frac{\partial n_p}{\partial \phi} = -\frac{1}{\phi^2}\left(n_{eff} - n_2\right)$$

This result clearly reveals i) that the variability of the retrieved values is different depending on both the concentration range and the RI contrast and, more importantly, ii) a large sensitivity in the dilute limit. This allows us to anticipate large variability in the retrieved data.

***Error propagation in the MG model*.** The same analysis can be done for other mixing rules, for instance, for the popular and widely accepted Maxwell-Garnett model, $\frac{\varepsilon_{eff}-\varepsilon_2}{\varepsilon_{eff}+2\varepsilon_2}=\phi\frac{\varepsilon_p-\varepsilon_2}{\varepsilon_p+2\varepsilon_2}$. In this case, the refractive index of the inclusions retrieved is $n_p=\left(\frac{1+2A}{1-A}\right)^{1/2}n_2=\left(\frac{\phi\left(n_{eff}^2+2n_2^2\right)+2\left(n_{eff}^2-n_2^2\right)}{\phi\left(n_{eff}^2+2n_2^2\right)-\left(n_{eff}^2-n_2^2\right)}\right)^{1/2}n_2$, from which the sensitivity terms can be evaluated as:

$$\frac{\partial n_p}{\partial n_{eff}}=9n_2^3n_{eff}\phi\left(\frac{\phi\left(n_{eff}^2+2n_2^2\right)+2\left(n_{eff}^2-n_2^2\right)}{\phi\left(n_{eff}^2+2n_2^2\right)-\left(n_{eff}^2-n_2^2\right)}\right)^{-1/2}\left(\frac{1}{\left[\phi\left(n_{eff}^2+2n_2^2\right)-\left(n_{eff}^2-n_2^2\right)\right]^2}\right)$$

$$\frac{\partial n_p}{\partial \phi}=\frac{1}{2}n_2\left(\frac{\phi\left(n_{eff}^2+2n_2^2\right)+2\left(n_{eff}^2-n_2^2\right)}{\phi\left(n_{eff}^2+2n_2^2\right)-\left(n_{eff}^2-n_2^2\right)}\right)^{-1/2}\left(\frac{-3\left(n_{eff}^2+2n_2^2\right)\left(n_{eff}^2-n_2^2\right)}{\left[\phi\left(n_{eff}^2+2n_2^2\right)-\left(n_{eff}^2-n_2^2\right)\right]^2}\right)$$

Here, although more convoluted, the inherent dependences $\frac{\partial n_p}{\partial n_{eff}}\propto\phi^{-1}$ and $\frac{\partial n_p}{\partial \phi}\propto\phi^{-2}$ are also present. This, again, allows anticipating large errors in the calculations at lower volume fractions, which happens to be precisely the range where a homogenization approach should work better.

***Error propagation in our measurements*.** The effective RI of the mixture is measured through the change in the Fresnel reflectivity (at normal incidence) with respect that of the solvent alone i.e., $n_{eff}\rightarrow n_{eff}(\Delta R,n_1)$. In the absence of both scattering and absorption, the DC voltage measured is proportional to the total power reflected from the fiber-medium interface i.e., $DC\propto P_T\propto I_T\propto R$, which is given by $R=\left|\frac{n_1-n_{eff}}{n_1+n_{eff}}\right|^2$, where n_1 if the effective RI of the MMF and n_{eff} is the effective RI of the medium where the fiber is immersed; the imaginary part of the complex RIs is zero. In the baseline measurement (solvent alone) $n_{eff}=n_2$.

If $n_1>n_{eff}$ is assumed at all times, as it is in our case, then the effective RI can be expressed as a function of the reflectivity measured as $n_{eff}=\left(\frac{1-\sqrt{R}}{1+\sqrt{R}}\right)n_1$. From this expression, it is obtained that $dn_{eff}=\frac{\partial n_{eff}}{\partial R}dR$, where $\frac{\partial n_{eff}}{\partial R}=-\left(\frac{1}{\sqrt{R}\left(1+\sqrt{R}\right)^2}\right)n_1$. Thus, the overall variability in the retrieval of the RI of dipoles through EMTs from on our fiber-based refractometric measurements can be expressed as:

$$dn_p=\frac{\partial n_p}{\partial \phi}d\phi+\frac{\partial n_p}{\partial n_{eff}}\frac{\partial n_{eff}}{\partial R}dR$$

The quantities $\frac{\partial n_{eff}}{\partial R}$ and dR appearing in the previous expression were measured experimentally using calibrated binary liquid mixtures of known RI (see Appendix C).

Detailed discussion and contextualization of our results. In order to put our results in perspective, we now discuss and compare them with other reports, specifically, those from Mershin A, et al [6] and Krivosudský et al [1].

Mershin A, et al [6] report a RI value for tubulin of n_{tub} = 2.9, which they obtained with two independent measurements of refractometry and surface plasmon resonances on tubulin suspensions. More recently, another experiment using refractometry performed by Krivosudský et al [1], suggested that this value should be around n_{tub} = 1.6. To understand the large discrepancies between the different results, including ours, we have summarized the main results and experimental details in Table S2.

Table S2. Summary of literature results concerning the refractive properties of tubulin in solution.

No.	A	B	C	D
References	Krivosudský et al [1]	Mershin A, et al [6a]	Mershin A, et al [6b]	Our results
Reported n	1.6	2.9	-	1.87
Reported slope: $\frac{\Delta n}{\Delta c}$ (10^{-3}mg/ml)	0.218±0.09	1.800±0.09	1.85±0.20	0.20
Approach	Refractometry	Refractometry	SPR	Reflectometry
Concentration range(mg/ml)	0-2	0-8	1.7-5.1	2-5
Temperature	25	-	26	21
Buffer	BRB80	MES	MES	BRB80+Colchcine+Glycerol
n of buffer	1.33654	1.3352	-	1.33864
pH	6.9	6.4	-	7.0
Sample volume (µL)	50	30-50	-	~900x10^{-6} (900 pL)

In previous reports, the effective RI of a tubulin suspension, n_{eff}, with certain concentration C_{tub}, is estimated by first measuring the slope of $n_{eff}(C_{tub},)$, in the concentration experiments, $\left(\frac{dn_{eff}}{dC}\right)$, assuming a known buffer i.e., $n_{eff} = \left(\frac{dn_{eff}}{dC}\right) C_{tub} + n_{buffer}$. From Table S2, it is clear that the large difference between the reported values of n_{tub} arises primarily from the different slopes measured. We found a number of different reasons for these large discrepancies at different levels, ranging from the sample preparation to the analysis of the data measured.

Sample preparation – possible existence of polymerized tubulin. In the experiments carried out by Mershin A, et al [6], the concentration of tubulin used is as high as 8 mg/ml. This concentration is above the critical concentration for polymerization and therefore spontaneous polymerization is prone to occur, even at room temperature [7]. Usually, when operating at a concentration that is higher than, or close to, the critical concentration (5 mg/ml), one needs to prevent polymerization and/or aggregation e.g., by adding colchicine and glycerol. No preventive measures were implemented in those reports. Furthermore, there is no supporting evidence of the lack of aggregates.

We verified the purity of samples prepared according to the standard protocol (without our preventive measures) and according to our modified protocol by independent measurements performed with a commercial DLS equipment (Malvern Zetasizer). We found out that in the case of the standard protocol tubulin clusters form systematically at room temperature with hydrodynamic size ranging from a few tens of nanometers to a few microns. Figure S2 shows typical results of the size distribution, by intensity and volume, obtained from the standard reports that are generated by the commercial DLS instrument. These distributions relate to the contribution to the scattering signal and the sample's composition, respectively.

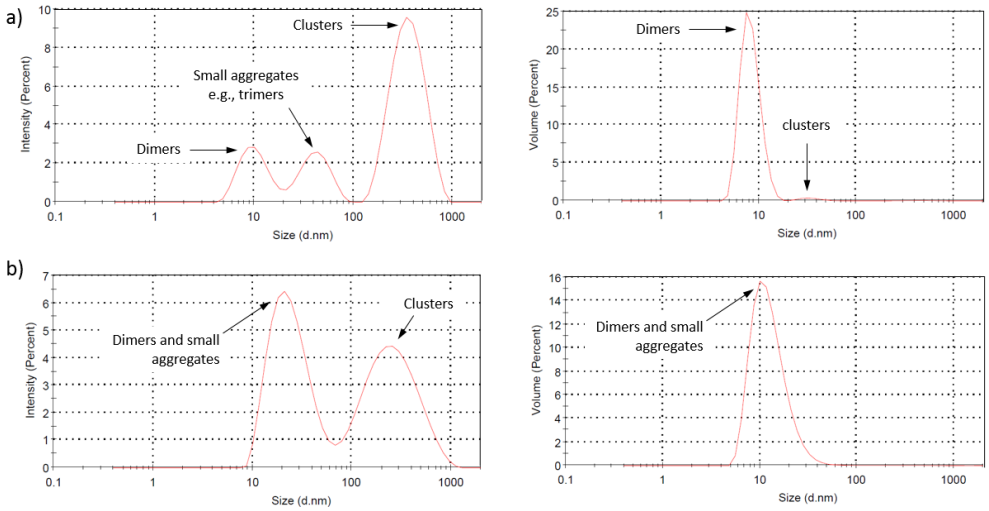

Figure S2. DLS measurement of samples prepared according to a) standard protocol, and b) our modified protocol in which preventive measures have been implemented in order to avoid the spontaneous formation of clusters. In b) both the composition and the optical measurement are dominated by tubulin dimers.

It can be seen that in both cases the composition is amply dominated by the population of dimers. However, in the case of the standard protocol the optical scattering signal is dominated by clusters which, besides inducing errors in the measurement due to significant scattering, compromises at a fundamental level the interpretation of the measurements within the frame of an effective medium. In our case, on the other hand, both the optical signal and the composition is dominated by dimers and residual small aggregates e.g., trimmers. It is important to recall that the DLS measurements are performed over a microliter-sized volume that is orders of magnitude larger than in our case (picoliters). In our much smaller volume, the distribution of populations shown in Figure S2(b) is not even well defined due to the scattering from the suspensions is comparable to that from the solvent alone, as explained in detail in Appendix C.

In terms of the data obtained in our measurement, with increasing aggregation we would see the progressive development of a power spectrum whose characteristic line width is associated to the average size of the aggregates, as in a traditional DLS measurement. In such case, the interpretation of the measurement in terms of an effective refractive index needs to be re-formulated in order to properly account for the scattering of the sample. More specifically, the effective refractive index becomes a complex quantity with an imaginary part that is associated to the losses due to scattering. When dealing

with even larger aggregates e.g., microtubules, the information retrieval is far more complicated since the complex refractive index needs to account, somehow, for the structural information of the aggregates (optical cross section).

Surprisingly, both papers [1, 6a] show measurements of the RI of tubulin MTs in suspension and the values reported are claimed to be similar to those of tubulin dimers in suspension! In the case of a suspension of MTs, the large dimensions of the cylinder, the presence of spatial correlation between dipoles, and the fact that a suspension of MTs constitute a situation where scattering cannot be neglected, forbid a straightforward use of EMTs due to the optical inhomogeneity of the system. As mentioned before, care should be exerted in the indiscriminate use of retrieving a value of refractive index through EMTs.

Accuracy in estimating the mass fraction $\boldsymbol{\chi = \frac{C_{tub}}{\rho_{sol}}}$**.** The density of the tubulin suspensions, ρ_{sol}, in the previous reports is claimed to be 1.45 and 1.41 g/ml, respectively. However, these values are too large, even for our case, where the aqueous suspension consists mainly of BRB80 buffer (we measured its density to be 1.0085 g/ml), 6 vol% of glycerol (1.26 g/ml), and a negligible contribution from tubulin and colchicine. In the previous reports, the origin of the value of ρ_{sol} is unclear.

The EMTs are based on volume fraction. Electromagnetic mixing models that describe an effective medium are developed in terms of volume fractions of specific components. In their work, the authors used mass fraction instead, which avoids involving the density of a tubulin dimer in the calculations. However, this approximation is reasonable for density-matched systems i.e., where the density of the particles is close to that of the solvent. Unfortunately, this is not the case. We estimated the density of a tubulin dimer, by using the molecular weight and the volume of a tubulin monomer to be, $\rho_{tub} = \frac{m}{V} = \frac{55kDa}{44nm^3} = 2.08 g/ml$, which is about two times larger than ρ_{sol}.

In order to illustrate the impact of the density contrast in the value of n_{tub} retrieved, we re-calculated the values in the previous reports using our value of ρ_{tub}. The results are summarized in Table S2.

Appendix C – Procedural details for the measurement of n_{eff}

Calibration measurements. For the calibration measurements, we used aqueous solutions of glycerol and ethylene glycol, with mass concentration in the range from 0 to 25 wt%. In both cases, the refractive index of binary mixtures with DI water follows a linear behavior [8]. These two different materials were used to produce scattering-free, homogeneous systems with RI around that of water with comparable values. At a free-space wavelength of 670 nm and room temperature of 21C, the RI of water [9], glycerol [10], and ethylene glycol [11] is 1.3386, 1.4695, and 1.4289, respectively. Thus, the refractive index of the solvents, for the range of concentrations explored (0-25 wt%), is modulated from 1.3310 to 1.3656 when using glycerol, and from 1.3310 to 1.3555 when using ethylene glycol.

The measurements were done in bulk systems by immersing the fiber in 500 µL of sample. The fiber was placed the center of the column of liquid, far from the bottom and lateral walls. The fiber was cleaved before starting to work with each set of solutions; the same optical fiber was used throughout samples of

the same set. The fiber was rapidly switched from sample to sample, from lower to higher concentration, in order to avoid the formation of residues at the tip of the fiber. After placing the fiber within the bulk, the system was let to stabilize for at least 5 min. Power spectra were recorded in the frequency range from 1 Hz to 10 kHz, with 1 Hz resolution and integration time of 30 s. For each solution, the total duration of the measurement was 5 min (10 spectra recorded per data point). Figure S3 shows the summary of the reflectivity measurements for these two systems.

The quantities dR and $\frac{\partial n_{eff}}{\partial R}$ appearing in the variational analysis, $dn_p = \frac{\partial n_p}{\partial \phi} d\phi + \frac{\partial n_p}{\partial n_{eff}} \frac{\partial n_{eff}}{\partial R}\, dR$, were measured experimentally using the above-mentioned calibrated binary liquid mixtures of known RI. The typical variability within a single data point i.e., at a single concentration, $dR = \sigma_R$, was measured experimentally and is $< 5 \times 10^{-3}$ at all times (Figure S3(a)).

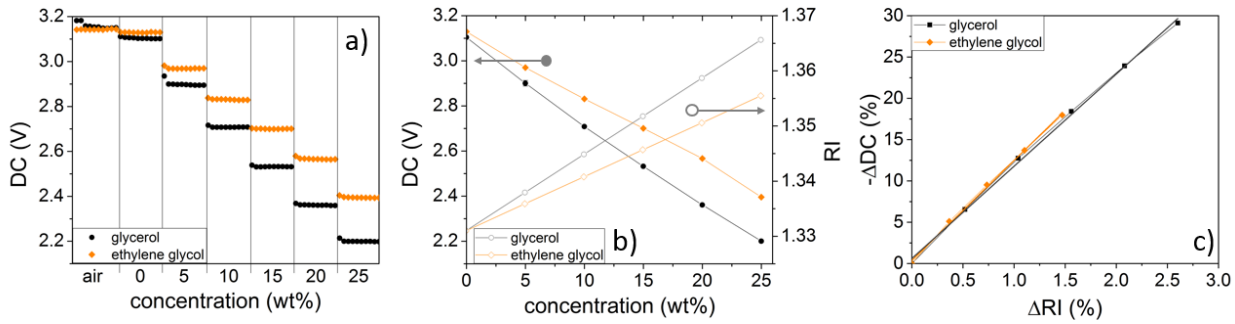

Figure S3. a) Raw measurement of reflectivity in the form of the time-averaged voltage measured by the detector for aqueous solutions of ethylene glycol and glycerol. From these plots, the typical variability in the reflectivity measurement (at a single concentration), dR, can be estimated. b) Average reflectivity (averaged over the raw measurements at each individual concentration in panel (a)) and corresponding effective RI of the aqueous solutions, according to Refs. [8-11]. c) Changes in the reflectivity produced by changes in the effective RI of the aqueous solutions. From this plot, the quantity $\frac{\Delta R}{\Delta n_{eff}} = \frac{1}{\frac{\partial n_{eff}}{\partial R}}$ can be estimated.

Strictly speaking, the dependence of the voltage measured on n_{eff}, and thus that of the Fresnel reflectivity i.e., $DC \propto R$, is quadratic (Figure S3(b-c)). However, a linear approximation is reasonable for a narrow RI range, far from the RI matching condition, corresponding to a large RI contrast between the fiber and the solution. It follows that the linear fits (Figure S3(c)) retrieve the value of $\frac{dR}{dn_{eff}} = \frac{\partial R}{\partial n_{eff}} = \frac{1}{\frac{\partial n_{eff}}{\partial R}}$ to be -11.167 for ethylene glycol systems and -12.113 for glycerol, respectively. This, in turn, results in $\frac{\partial n_{eff}}{\partial R} = 0.086$ on average from these two independent experiments. Thus, the precision in the measurement of n_{eff} corresponding to the maximum variability can be estimated to be $dn_{eff} = \frac{\partial n_{eff}}{\partial R} dR \approx (1 \times 10^{-1})(5 \times 10^{-3}) = 5 \times 10^{-4}$.

This value is comparable to that of commercial refractometers. We should note, however, that the source for sensitivity is different in both cases. In the case of a commercial refractometer, the sensitivity is mainly

determined by the angular resolution in the measurement of the refracted beam (see Appendix B). In our case, it is dictated by the resolution in the measurement of reflectivity (the time-averaged total intensity).

By using the same approach described in the main text, the RI of the pure solutes i.e., glycerol and ethylene glycol, retrieved at 670nm, 21C, are **1.4461 ± 0.0021** (compare to the value in Ref. [10], of 1.4695) and **1.4178 ± 0.0033** (compare to the value in Ref. [11], of 1.4289), respectively. The standard deviation was obtained from the values retrieved across the different solutions.

Finally, we also verified that the negligible-scattering condition is satisfied at all times as the spectra recorded for the different solutions are practically the same as that of the water alone (Figure S4). The spectral content, in all cases, is dominated by the electronic and environmental noise of the detection system.

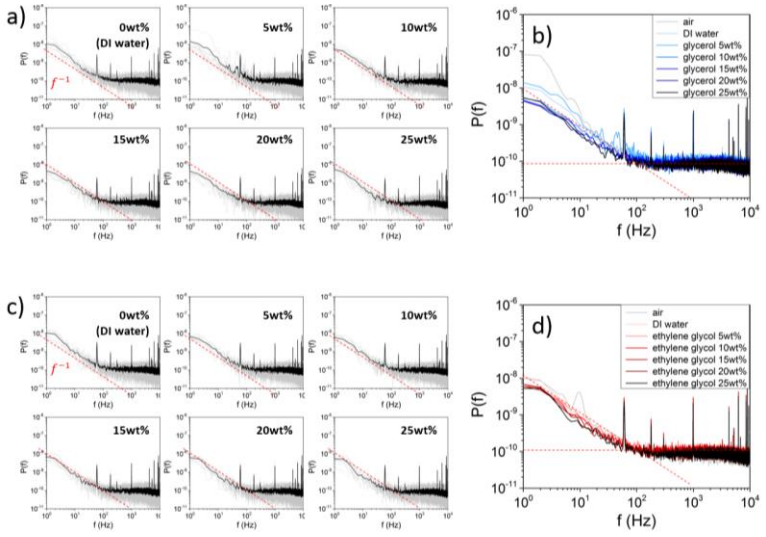

Figure S4. Collection of the raw (left panels, a) and c)) and averaged (right panels, b) and d)) power spectra measured for aqueous solutions of a)-b) glycerol and c)-d) ethylene glycol. The slope of -1 in the logarithmic scale of the plots indicates the typical spectral dependence of the electronic (shot) noise of the detector. The horizontal dashed line indicates the environmental noise floor of our detection system.

Measurements on tubulin systems. We also verified that the negligible-scattering condition is satisfied at all times for the tubulin systems testes. In Figure S5, we show the raw and average power spectra for tubulin suspensions with different concentrations the different solutions.

These results illustrate the main advantage of our experimental implementation: the ability to perform, simultaneously, refractometric measurements and dynamic scattering examination of the medium under test. In this regard, commercial refractometers do not provide means to assess the scattering of the sample (neither dynamic nor static). Basically, the information retrieval relies on the assumption that the sample is scattering-free, which is impossible to verify in real time using traditional refractometric techniques.

This can lead to errors in the values of the refractive index retrieved because, in the presence of scattering, the effective medium depiction should comprise a complex refractive index (see detailed discussion above, around Figure S2). The fact that we can assess dynamic scattering of the sample in situ is of great value i) to verify the validity of an effective medium model, ii) to make proper adjustments to the effective medium model used, if necessary, and ultimately, iii) to ensure that the information retrieval is correct. In the particular case of dilute samples where no aggregation takes place i.e., weak scattering, the *in situ* measurement of dynamic scattering is used only to verify that the measurements are properly framed within an effective medium interpretation.

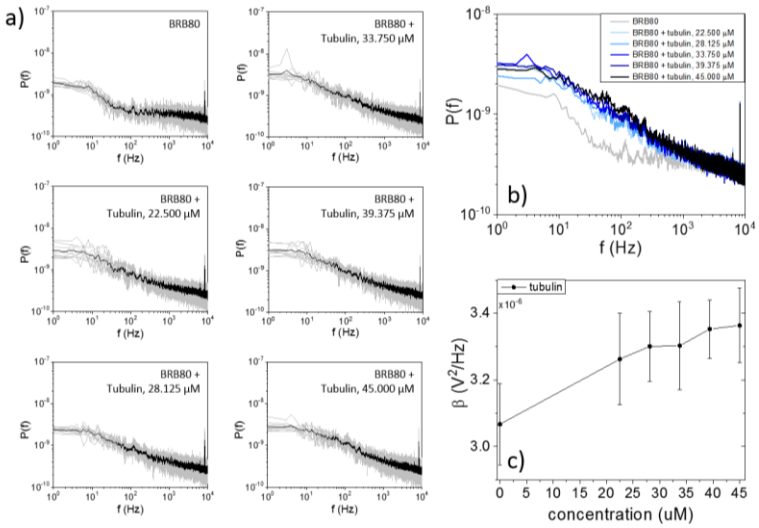

Figure S5. Collection of the a) raw and b) average power spectra measured for aqueous suspensions of tubulin with different concentration, and c) their associated total scattered energy, β.

Appendix D – Procedural details for the numerical computations

Tubulin model

The atomic coordinates for the tubulin dimer were obtained from the Protein Data Bank (PDB ID: 1JFF [12]). The coordinates for the missing residues α:1, β:1, and α:35–60 were obtained by modeling with the Molecular Operating Environment (MOE) software package [13]. This C-terminus has not been included in the electron crystallography data of the PDB structure due to its flexibility, so all calculated dipole moment values are *stated* ignoring the effects of the C-terminus. The missing hydrogens for heavy atoms were added using the tLEAP module of AMBER 14 [14] with the AMBER14SB force field. The protonation states of all ionizable residues were determined at pH = 7 using the MOE program. Each protein model was solvated in a 12 Å box of TIP3P water. In order to bring the salt concentration to the physiological value of 0.15 M, 93 Na^+ ions and 57 Cl^- ions were added. After minimization, the molecular dynamics (MD) simulations were carried out in three steps: heating, density equilibration, and production. First, each solvated system was heated to 300 K for 50 ps, with weak restraints on all backbone atoms. Next, density equilibration was carried out for 50 ps of constant pressure equilibration at 300 K, with weak restraints. Finally, MD production runs were performed on all systems for 100 ns. The largest cluster conformation

of the tubulin structure from the production simulations was used for all further calculations in the study. The crystal structure contained 1 taxol, 422 amino acid residues, 1 GTP, and 1 Mg^{2+} in α-tubulin; 426 amino acid residues, and 1 GDP in β-tubulin. For further calculations, the taxol molecule, GTP, and GDP and the Mg^{2+} were all removed from the complex after equilibration.

Permanent dipole moment and charge at different pH levels. To simulate the structure of tubulin at different pH levels, the Protonate3D module of MOE [13] was employed to calculate the optimal protonation states, including titration, rotamer, and flips using a large-scale combinatorial search. Prior to computing the protein descriptors (dipole moment and net charge), partial charges were assigned to all atoms using the AMBER 12 force field. The charges on individual residues were set with the use of the Henderson-Hasselbalch equation [15], given their estimated pK_a values based on the PROPKA method [16]. This ensured a zero net charge at the isoelectric point and allowed for smooth transitions as the pH level was varied. The permanent dipole moment of the tubulin was computed at a given pH-appropriate protonation state across a range of pH values pH = [6.5,7.5] and ionic strengths I = [17] M with T = 293 K, a friction coefficient of η = 0.00089 Pa·s, and a solvent dielectric constant of ε_r = 78 using the protein property calculator module of the MOE software employing the following formula: $p = 4.802 \sum_i^N q_i r_i$.

Polarizability calculations. We used semi-empirical QM method to calculate the static polarizability (zero frequency) of the tubulin dimer. All geometries used during this investigation were optimized using the PM6 Hamiltonian, BFGS optimizer, and the MOZYME method using MOPAC2016 [18]. The MOZYME method [19] uses localized orbitals to solve the self-consistent field (SCF) equations, making possible QM calculations to study larger systems such as entire proteins with several thousand atoms. To calculate the static polarizability, an electric field gradient (0.10284 volts per Ångstrom ~ 10^9 V/m) was applied to the system to evaluate the effect on the calculated heat of formation and on the dipole. The polarizability, it should be noted, can be evaluated from the change in dipole moment or the heat of formation. A measure of the precision of the calculation can be obtained by comparing the polarizability calculated by the two methods. In static calculations, the polarizability involved 36 scf calculations, one for each electric field (+X, −X, +2X, −2X, +Y, −Y, +2Y, −2Y, +X+Y, −X+Y, …). These were used in the construction of a three-by-three secular matrix, which was then diagonalized, giving the orthogonal polarizabilities. COSMO implicit solvent was used to simulate an aqueous environment with the liquid phase dielectric constant of 78.4. The calculated polarizability at pH = 6.9 was found to be approximately 1.13×10^{-36} using the dipole moment approach. It should be mentioned that the various methods in MOPAC all underestimate the polarizability by about 50%.

An estimation of tubulin polarizability. A simplified estimate of tubulin polarizability $\propto = \frac{\Delta p}{\Delta E}$ can be done in terms of Δp , the induced dipole moment, and E the externally applied electric field (EEF) acting on the protein. Once the tubulin dimer interacts with the electric field, there will essentially be four different additive contributions to the induced dipole moment as follows.

1) Δp_1 is due to the stretch in the permanent dipole moments of the protein's polar amino acids aligned with the electric field,

2) Δp_2 is due to the displacement of positive and negative charges of the charged amino acids moving under the effect of the electric field,
3) Δp_3 is due to the displacement of counter ions congregated at the C-termini of the tubulin dimer as a result of moving in the electric field, and
4) Δp_4 is due to the organization of water molecules at the solvation shell around the tubulin dimer as an effect of the electric field.

Atomistic simulations of different proteins in EEFs have demonstrated that protein dipoles are affected by the localized rearrangement of charged side chains and loops [20]. Dipole moment can be modeled as a two-charge object, $-q$ and $+q$, of equal magnitude and opposite sign, separated by distance d using $\Delta p = \sum_{i=1}^{4} q_i d_i$ (Eq. 3) considering the four contributions described above. The four contributions can be calculated as follows:

(1) Δp_1 can be estimated by assuming an elongation of the dipole moment of tubulin. According to the results of the Molecular Dynamics (MD) simulations studying the effect of EEFs on tubulin, the EEF doubled the magnitude of the tubulin's dipole moment [21], so $\Delta p_1 =$ (~20% × 2000 D = 400 D), which will be 400 D. The calculated dipole moment at pH = 6.9 is approximately 1970 (see Figure 1). So $\Delta p_1 = 4 \text{´} 10^{2} \text{´} 3 \text{´} 10^{-30} = 1.2 \times 10^{-27}$ Cm, considering the conversion unit as 1 D = 3.3×10^{30}Cm

2) Δp_2 can be estimated by considering the displacement of the charged amino acid residues (lysine (+), arginine (+), aspartate (−) and glutamate (−)) in tubulin due to the effect of EEF. The distance can be approximated from RMSD results of MD calculation studying the effect of EEFs on tubulin as 2 Å [21]. The calculated charge at pH = 6.9 is approximately −34 (see Figure 1). Therefore, $\Delta p_2 = (34 \times 1.6 \times 10^{-19}) \times 4 \times 10^{-10} = 2 \times 10^{-27}$ Cm, considering the displacement of 4 Å.

3) Δp_3 can be calculated considering the fact that the counter ions at C-terminal (~20 ions) can be displaced by the Debye wavelength $\lambda_D = 10^{-9}$. As such, Δp_3 will be $\Delta p_3 = (20 \times 1.6 \times 10^{-19}) \times 10^{-9} = 3 \times 10^{-27}$Cm

4) To estimate Δp_4, we approximated the number of water molecules in the solvation shell around the tubulin by assuming that each tubulin monomer can be considered as a sphere with an R = 20 Å dimeter. An approximation for the volume of a thin spherical shell is the area of the outer sphere multiplied by the thickness of the shell. The thickness of the shell can be estimated from a typical radial distribution function g(r) calculated from molecular dynamics simulations for a tubulin monomer where g(r) = 1 (dr =4 Å). Total number of water molecules can be calculated as

$$\frac{volume\ of\ the\ shell}{volume\ of\ the\ water\ molecule} = 2 \times \frac{4\pi R^2 dr}{4\pi r^2} = 2 \times \frac{4\pi \times (20)^2 \times 4}{4\pi (1.4)^2} \sim 1{,}600$$

Considering the volume of two tubulin monomers comprising one dimer, the volume of the shell is multiplied by 2. We consider the radius of the water molecule as r = 1.4 Å. Then Δp_4 can be calculated as $\Delta p_4 = 1{,}600 \times (1.8 \times 3.3 \times 10^{-30}) = 9.5 \times 10^{-27}$, where the dipole moment of water is 1.8 D.

Thus, the total dipole moment, Δp, can be calculated by adding all the contributions using: $\Delta p = \Delta p_1 + \Delta p_2 + \Delta p_3 + \Delta p_4 = 15.7 \times 10^{-27} = 1.5 \times 10^{-26}$. As the EEF used in the computational experiments ranged from 50 kV/cm to 750 kV/cm (0.05 to 0.75 x 10^8 V/m), the polarizability therefore can be calculated

for the middle of this range (400 kV/cm) using Eq. 2 as: $\alpha = \frac{\Delta p}{E} = \frac{15.7\times10^{-27}}{0.4\times10^{8}} = 3.93 \times 10^{-34}$ which falls within the range of values shown in Figure 3 of the main text, namely 3 to 9 x 10^{-34}. Since the above estimation is obtained at a constant electric field as opposed to the response of the system to the visible range of electromagnetic radiation, our simplified model provides a fairly good insight into the system's behaviour.

References

1. Krivosudský, O.; Dráber, P.; Cifra, M., Resolving controversy of unusually high refractive index of a tubulin. *EPL (Europhysics Letters)* **2017,** *117* (3), 38003.
2. Sihvola, A., Mixing rules with complex dielectric coefficients. *Subsurface sensing technologies and applications* **2000,** *1* (4), 393-415.
3. Lorentz, H., Ueber die Anwendung des Satzes vom Virial in der kinetischen Theorie der Gase. *Annalen der physik* **1881,** *248* (1), 127-136.
4. Wiener, O., Mathematisch-Physikalische Klasse. *Leipziger Berichte* **1910,** *62*, 256.
5. Heller, W., Remarks on refractive index mixture rules. *The Journal of Physical Chemistry* **1965,** *69* (4), 1123-1129.
6. (a) Mershin, A.; Kolomenski, A. A.; Schuessler, H. A.; Nanopoulos, D. V., Tubulin dipole moment, dielectric constant and quantum behavior: computer simulations, experimental results and suggestions. *Biosystems* **2004,** *77* (1-3), 73-85; (b) Schuessler, H. A.; Mershin, A.; Kolomenskii, A. A.; Nanopoulos, D. V., Surface plasmon resonance study of the actin-myosin sarcomeric complex and tubulin dimers. *journal of modern optics* **2003,** *50* (15-17), 2381-2391.
7. Engelborghs, Y.; Heremans, K. A.; DE MAEYER, L. C.; HOEBEKE, J., Effect of temperature and pressure on polymerisation equilibrium of neuronal microtubules. *Nature* **1976,** *259* (5545), 686.
8. Haynes, W. M., *CRC handbook of chemistry and physics*. CRC press: 2014.
9. Daimon, M.; Masumura, A., Measurement of the refractive index of distilled water from the near-infrared region to the ultraviolet region. *Applied optics* **2007,** *46* (18), 3811-3820.
10. Rheims, J.; Köser, J.; Wriedt, T., Refractive-index measurements in the near-IR using an Abbe refractometer. *Measurement Science and Technology* **1997,** *8* (6), 601.
11. Sani, E.; Dell'Oro, A., Optical constants of ethylene glycol over an extremely wide spectral range. *Optical Materials* **2014,** *37*, 36-41.
12. Löwe, J.; Li, H.; Downing, K. H.; Nogales, E., Refined structure of αβ-tubulin at 3.5 Å resolution11Edited by I. A. Wilson. *J Mol Biol* **2001,** *313* (5), 1045-1057.
13. Chemical Computing Group. (2012). Molecular Operating Environment (MOE), S. S. W., Suite #910, Montreal, QC, Canada, H3A 2R7.
14. D.A. Case, R. M. B., W. Botello-Smith, D.S. Cerutti, T.E. Cheatham, III, T.A. Darden, R.E. Duke, T.J. Giese, H. Gohlke, A.W. Goetz, N. Homeyer, S. Izadi, P. Janowski, J. Kaus, A. Kovalenko, T.S. Lee, S. LeGrand, P. Li, C. Lin, T. Luchko, R. Luo, B. Madej, D. Mermelstein, K.M. Merz, G. Monard, H. Nguyen, H.T. Nguyen, I. Omelyan, A. Onufriev, D.R. Roe, A. Roitberg, C. Sagui, C.L. Simmerling, J. Swails, R.C. Walker, J. Wang, R.M. Wolf, X. Wu, L. Xiao, D.M. York and P.A. Kollman *AMBER 2014*, University of California, San Francisco., 2014.
15. Cameselle, J.; Meireles Ribeiro, J.; Sillero, A., Derivation and use of a formula to calculate the net charge of acid-base compounds. Its application to amino acids, proteins and nucleotides. *Biochemical Education* **1986,** *14* (3), 131-136.
16. Li, H.; Robertson, A. D.; Jensen, J. H., Very fast empirical prediction and rationalization of protein pKa values. *Proteins: Structure, Function, and Bioinformatics* **2005,** *61* (4), 704-721.
17. The role of DNA twist in the packaging of viral genomes. *Biophys. J.* **2008,** *94*, L38.
18. MOPAC2016, J. J. P. S., Stewart Computational Chemistry, Colorado Springs, CO, USA, HTTP://OpenMOPAC.net (2016).
19. Stewart, J. J. P., Application of localized molecular orbitals to the solution of semiempirical self-consistent field equations. *International Journal of Quantum Chemistry* **1996,** *58* (2), 133-146.

20. (a) Budi, A.; Legge, F. S.; Treutlein, H.; Yarovsky, I., Electric field effects on insulin chain-B conformation. *J Phys Chem B* **2005,** *109* (47), 22641-22648; (b) English, N. J.; Solomentsev, G. Y.; O'Brien, P., Nonequilibrium molecular dynamics study of electric and low-frequency microwave fields on hen egg white lysozyme. *The Journal of Chemical Physics* **2009,** *131* (3), 035106; (c) Budi, A.; Legge, F. S.; Treutlein, H.; Yarovsky, I., Effect of frequency on insulin response to electric field stress. *J Phys Chem B* **2007,** *111* (20), 5748-5756.
21. Timmons, J. J.; Preto, J.; Tuszynski, J. A.; Wong, E. T., Tubulin's response to external electric fields by molecular dynamics simulations. *PLOS ONE* **2018,** *13* (9), e0202141.